Title
Protein Half-life of Degradation Machineries in Healthy and Stressed Myocardium

Author
Polson, Jennifer Sara

Publication Date
2017

Peer reviewed|Thesis/dissertation

UNIVERSITY OF CALIFORNIA

Los Angeles

Protein Half-life of Degradation Machineries in Healthy and Stressed Myocardium

A thesis submitted in partial satisfaction

of the requirements for the degree

Master of Science in Physiological Science

by

Jennifer Sara Polson

2017

ABSTRACT OF THE THESIS

Protein Half-life of Degradation Machineries

in Healthy and Stressed Myocardium

by

Jennifer Sara Polson

Master of Science in Physiological Science

University of California, Los Angeles, 2017

Professor Rachelle Hope Watson, Co-Chair

Professor Peipei Ping, Co-Chair

Protein synthesis and degradation function in concert to maintain myocardial proteome homeostasis and render proteome dynamics triggered by pathological stresses; mounting evidence documents their dysfunction as a cardiac disease driver. Despite our knowledge of hypertrophic signaling cascades in heart, little is known about the concomitant self-regulation of protein synthesis and degradation machineries during this proteome-wide remodeling. For 6 genetic mouse strains that developed distinguishable scales of ISO-induced hypertrophy, the basal and altered protein half-lives were quantified for proteasomal subunits as well as other degradation and synthesis machineries. Contractile proteins were quantified as half-life references to hypertrophy. The workflow developed in this study revealed the unique turnover features among six genetic strains, the distinct turnover modulation of individual proteasomal subunits under β-adrenergic stimulation, and a signature of contractile protein turnover alteration. Together with functional assessments, our discovery supports future investigations to dissect these regulatory processes in maladaptive cardiac remodeling.

The thesis of Jennifer Sara Polson is approved.

Xia Yang

Peipei Ping, Committee Co-Chair

Rachelle Hope Watson, Committee Co-Chair

University of California, Los Angeles

2017

Table of Contents

List of Tables and Figures

Acknowledgments

I wish to acknowledge my mentor, Dr. Peipei Ping, and all members of the Ping Lab for their invaluable guidance and assistance during my time in the Master's Program. I'd also like to acknowledge the members of my thesis committee for their time and effort during the thesis preparation and approval process. Finally, I'd like to acknowledge and thank my family and friends for their endless support and encouragement.

Introduction

Despite a wealth of research, cardiovascular disease remains the leading cause of death among populations in the United States.[1] This high rate of mortality may be attributed to irreversible deterioration of cardiac structure and function caused by long-term, detrimental molecular alterations to cardiac tissue, which hinder the development of effective therapeutic strategies. Proteolytic machineries, specifically the proteasome, have been implicated as a driver of many cardiovascular diseases;[2] the rate of synthesis and degradation, or turnover, of the proteasome illustrates one novel facet of the complex interplay of molecular components and their resulting governance of phenotype. This study sought to characterize the effect of hypertrophic stimulation on proteasomal subunit turnover, and determine the resulting consequences on contractile proteins within cardiomyocytes. Analytics metrics were developed to unveil the behavior of biological protein groups; by assessing proteasome machineries in the context of other turnover protein species, as well as contractile unit proteins, statistical methods reveal the subunits most sensitive to hypertrophic stress, and a cardiac signature of induced pathological hypertrophy.

Prolonged stresses on the heart can induce many forms of pathological conditions, including cardiac hypertrophy, which can precede or exacerbate severe cardiac events and may critically inhibit successful cardiac outcomes.[3] Cardiac hypertrophy is characterized by a thickening of the cardiac muscle wall, most often as an adaptive response, in the ventricular myocardium. Ventricular hypertrophy can be classified into two types: physiological and pathological. Hypertrophic growth in response to cardiovascular training is typical of physiological cardiac remodeling, and can be beneficial, such as observed in the hearts of endurance athletes.[4 5] Often termed exercise-induced hypertrophy, it differs in its molecular profile to pathological hypertrophy**,** the maladaptive physical manifestations of which are considerably more severe.

Cell enlargement, augmented sarcomeric assembly, and an increased rate of protein synthesis are emblematic of pathological hypertrophy at the cellular level.[6] At the organ level, pathophysiological remodeling mechanisms create two distinct subtypes of cardiac hypertrophy: concentric hypertrophy results as a response to heightened pressure load, in which the ventricular cardiomyocytes grow toward the center of the ventricle, and is marked by additional sarcomeres in parallel and therefore lateral cell growth for compensatory force generation, and; eccentric hypertrophy in response to high volume or infarction, which results in increased sarcomeres in series to increase contractile velocity as well as longitudinal cell growth.[7]

The long-term administration of isoproterenol (ISO) within mammalian model systems produces cardiac hypertrophy pathology; ISO is a non-specific β-adrenergic agonist, and binds to the β_1 adrenoreceptor, a G-protein coupled receptor in the heart. Many studies have concluded that dysfunction of the β_1-adrenergic receptor system propels the heart into maladaptive remodeling and results a pathological phenotype.[3] After activating the PI3K/AKT signaling pathway, an increase in cAMP within cardiomyocytes has an effect specific to cardiac muscle.[8] Through both its inotropic and chronotropic effects, ISO induces increased firing rate in the sinoatrial node, amplified conduction autorhythmicity through to cardiac muscle, and enhanced contractility. This heightened cardiac output eventually produces eccentric hypertrophy and dilated cardiomyopathy. Large doses of ISO stimulation cause vascular contraction and ischemic damage, in addition to hypertrophic effects; a low dose of ISO is sufficient to elucidate hypertrophic effects without confounding factors associated with ischemic injury or severe heart failure.[9]

Multiple factors underlie the progression of cardiac hypertrophy into heart failure or other cardiac events. Decades of Cardiovascular research has illustrated that many pathways and proteins underlie the pathological manifestation of adverse cardiac phenotypes. Despite this key evidence, there still lacks a global understanding of the complex interplay of genes, proteins, and small molecules, and their network interactions that impact cardiomyocyte health. With the

advent of genomics, scientists developed untargeted approaches to finding differences in the genetic makeup of individuals and the effects on their phenotypes. Indeed, these studies led to the discovery of many Mendelian genetic markers for disease.[10] [11] These studies and high-throughput approaches have paved the way for other omics approaches to take hold, such as transcriptomics, proteomics, and metabolomics. While genetic markers have been identified via genomics studies, it is becoming increasingly apparent that cardiovascular disease is a multifactorial disorder, and multi-dimensional omics strategies are needed to be integrated and tailored for providing the most elucidative information.[12] As cellular functions are substantiated by an interactive network of cellular proteomes, studying the entire pool of proteins within a cell via proteomics methods can provide key insights into gene expression, as the proteome is stable, but still sensitive enough to experience alterations under cellular stress.

Within proteomics, two major parameters are used to define individual protein species of a proteome: protein expression and protein turnover. Protein expression is the steady-state quantification of a protein at a specific time point. Protein turnover rate, or half-life, integrates information over multiple time points to provide information about the interplay of protein synthesis and degradation of a specific protein.[13] Indeed, the mechanisms underlying many diseases reveal proteostatic measurements, resulting in measurements lacking observable change in the quantified steady-state expression level of a particular protein. The temporal dynamics can be better observed by measuring the turnover rate, of proteins under various experimental conditions.[14] Proteomics studies of turnover rate have correlated protein pool variations with causative mechanisms for such conditions as neurodegeneration and cardiovascular diseases.[15] [16]

Despite the invaluable utility found in large-scale protein turnover profiles, the number of such datasets remains scarce, as there are many technical barriers to accurately measuring protein turnover. Since first mention of the concept in 1935, there have been a few well-developed methods, though they are not without their drawbacks. Dynamic Stable Isotope

Labeling by Amino Acids in Cell Culture (SILAC) has been used to measure incorporation of amino acids,[17] but this does not fully encapsulate *in vivo* protein studies. For *in vivo* studies, experimenters have used synthetic amino acids in diets of animals, but altering the diet could confound factors for certain studies, and the specialized chow is costly.[18] More recently, a novel method involving deuterium oxide (^2H_2O) labeling has been developed. By providing animals with ^2H_2O-enriched drinking water, the gradual incorporation of the hydrogen isotope can be measured and modeled into the turnover rate for that protein.[16 19 20] To automate the half-life quantification directly from MS raw data, our group developed ProTurn, a software program that reads mass spectra and protein identification and provides a unified, curve-fitting kinetic model.[21] This method is safe, less expensive than previous methods, and easier to apply across a variety of model systems, making it a highly viable strategy for determining the turnover rates of an entire proteome.

Within a proteome, an individual protein's turnover rate is the amalgamation of the activities of many protein synthesis and degradation machineries. Proteins responsible for synthesis primarily consist of ribosomal complex subunits and transcription factors, while protein degradation is regulated by a complex set of contributors including the ubiquitin-proteasome system, the autophagy/lysosome system, and individual peptidases or proteases.[22] Within the heart, proteasomes are essential to maintaining myocardial proteome homeostasis; mounting evidence documents their dysfunction as a cardiac disease driver. Indeed, proteasome inhibitors have been identified as drug targets during restrictive cardiomyopathy,[23 24] but this general inhibition produces unwanted side effects such as cardiotoxicity. One potential area for discovery might be to target specific proteasomal components to alter the complex function.

The proteasome is made up of a 20S core particle (CP) and 19S regulatory particle (RP). The CP comprises four stacked rings with seven proteins each, forming a pore in the middle. The inner rings have 3-7 protease active sites, and are responsible for the enzymatic degradation of the entire complex, while the outer rings contain α-subunits that act as a gating

mechanism for the pore.[25] The RP recognizes the ubiquitin tags attached to proteins, and determines if the protein is ready for degradation; if so, the RP initiates the protein degradation process by localizing the protein to the CP.[26] [27] Proteasomes are an integral component of the Ubiquitin-Proteasome-System, specifically responsible for protein quality control.[28] Ubiquitin tagging and subsequent proteolysis regulates the cell cycle, cell growth, differentiation, gene transcription, signal transduction, and programmed cell death via apoptosis.[29] The regulation of the cytosolic proteasome is complicated, supported by multidimensional molecular processes including expression of individual subunits, assembly of the complex, recruitment of heterogeneous subunits or subcomplexes, associating partners, and post-translational modifications; in addition, recent studies in protein turnover validate it as another layer of regulation.[30] However, there is a dearth of knowledge regarding the concerted interplay of these molecular processes in response to pathological challenges, necessitating a systematic characterization of proteasomal subunit turnover while under stress.

In studying the pathological mechanisms driving cardiac diseases, it has become apparent that the heart must maintain molecular homeostasis while providing sufficient physical activities as fundamental cardiac output, in order to meet the demands for maintaining cell functions and even cell survival in response to a wide variety of physiological stressors and injury over time. Characterizing the potential self-regulatory capacity of the proteasome can provide distinctive insight, but this must be taken in context of other synthesis and degradation machineries to determine the contribution of both arms of protein turnover regulation. Moreover, to achieve a truly comprehensive understanding, these turnover rates should then be compared to the functional targets of the machineries, namely contractile proteins, to provide a relative reference point. Therefore, this study aimed to assess the unique regulation of proteasome subunit turnover under ISO-induced stress conditions across multiple model system strains, and ascertain the downstream effects of protein turnover machineries on functional contractile protein turnover. This workflow involved visualizing protein turnovers and calculating qualitative

measurements to represent biological parameters, using statistical methods to determine differential responses of both functional groups and individual subunits across six strains, and applying methods to identify a signature of contractile protein response to ISO. The proteasomal complex exhibits a unique distribution of half-lives when compared to other synthesis and degradation machineries, as well as the entire proteome. Individual proteasomal subunits had differing turnover adjustment in hypertrophic conditions, with two protein species exhibiting significantly sensitive responses. Within the characterization of contractile machineries, ten proteins have markedly modulated half-lives. Integration of the knowledge presented here with protein expression data, or other omics methods, may provide a more complete picture of the interplay between protein turnover machineries and cardiac hypertrophy.

Materials and Methods

Dataset Generation Workflow: Labeling and Sample Collection

The data used in this study was previously generated as part of a landmark dataset for sustainable utility. Briefly, the following six mouse genetic strains were used for their wide applicability to cardiovascular, metabolic, cancer, and other studies, as well as their stratified susceptibility to β-adrenergic stimulated hypertrophy: FVB/nJ, CE/J, C57BL/6J, DBA/2J, BALB/cJ, and A/J. The mice were all juvenile males between 9-12 weeks of age. The mice received two 500 µl doses of 99.9% saline $^{2}H_2O$ (molar ratio) via intraperitoneal injection, and then were given access to 7.25% $^{2}H_2O$ (molar ratio) for the remaining duration of the study. Two mice were euthanized for each experimental group at the following time points: 0, 1, 3, 5, 7, 10, and 14 day(s); heart and plasma samples were collected from each group. In addition, mice undergoing isoproterenol treatment were given 15 $mg*kg^{-1}*d^{-1}$ via osmotic pump through the course of the study, totaling up to 14 days.[31]

Dataset Generation Workflow: Processing and Mass Spectrometry

$^{2}H_2O$ enrichment was determined via gas-chromatography mass spectrometry (GC-MS) on the mouse plasma samples from every experimental group. To extract cardiac-specific proteins, each sample was homogenized and fractionated to separate the nuclear/extracellular (nuclear), organelle-depleted (cytosolic), and mitochondrial/microsomal (mitochondrial) fractions. These fractions underwent further fractionation and digestion protocols to prepare each fraction for liquid chromatography-tandem mass spectrometry (LC-MS/MS). This form of mass spectrometry required reverse-phase chromatography for optimal peptide separation, followed by high-resolution tandem mass spectrometry. Proteins were inferred from peptide identification using ProLuCID algorithm against the UniProt database,[32] converting the raw .mzml to a tabular data format (.dta).

Dataset Generation Workflow: Determination of Protein Turnover Rate

From this identified data, ProTurn software determined the turnover rate using a novel strategy based in previously validated kinetic models.[20] After finding corresponding peptide peaks in each of the raw data files, peptide isotope incorporation via ^2H_2O-labeling was quantified by integrating isotopomer peak distribution. These quantifications were correlated to a time-series based on the collected time-points: the output was a table of isotope fractional abundances as a function of time. Finally, this time-series data was fitted to a non-linear kinetic model using a non-steady-state fitting method, from which the peptide turnover rate was computed using first-order kinetics. The resulting dataset comprises over 3200 quantified protein turnover rates for the six genetic mouse strains in control and isoproterenol conditions, and is available at: http://dx.doi.org/10.7303/syn4847184.2.[31]

Data Curation and Extraction

From the previously published protein turnover dataset, revant turnover rates were extracted for four protein functional clusters. Protein lists detailing applicable functional classes were extracted from UniProt and relevant selected literature,[33] including proteasomal proteins, non-proteasomal degradation proteins, and ribosomal proteins as an indicator of protein synthesis. A protein list was also generated for contractile proteins. These proteins were compared to lists found in previous publications; this information was integrated into final lists, which are detailed in Tables 1-4. For each of the six genetic mouse strains, a list was generated of the relevant proteins for which there were turnover rates for both the control and ISO conditions; the numbers of proteins found in the dataset for each these lists are summarized in Table 5. For this study, the half-lives of individual proteins were calculated from the k-values, or rate constants, found in the previously published dataset. The k-values were determined from first-order kinetic modeling; as such, half-life ($t_{1/2}$) can be calculated from k from the following equation.

$$t_{1/2} = \frac{\ln(2)}{k}$$

Data Representation

Three graphing methods were used to represent turnover data. To visualize the two-dimensional distribution of protein turnover, half-lives are plotted in control and ISO conditions on the x-axis and y-axis, respectively. For clarity, a line y=x was drawn on each plot to indicate zero alteration. The resulting scatter plot contains information about the biological behavior of a protein group. A protein's location on the plot indicates its behavior under hypertrophic stimulation: a protein that is resilient in response to ISO will lie on the zero alteration line, while a protein with increased turnover will lie under the zero-alteration line, and a protein with decreased turnover will lie above the zero-alteration line. Secondly, violin plots were assembled to illustrate the distribution of proteasomal and contractile cluster data in comparison to the entire proteome. The violin plots for a selected functional cluster are laid over those of the total proteome for each genetic strain; middle lines denote the median for each group. Finally, volcano plots were created by plotting $\log_2$(fold change) on the x-axis, and the $-\log_{10}$(p-value) on the y axis.

Metrics and Strategy

The quartile ranges of half-lives provide information about the distribution of turnover ranges within a protein group, indicating the degree of synchronized turnover among components within a functional group, summarized in Table 6. However, as the distributions do not illustrate the changes of an individual protein in response to turnover, other metrics can be used to compare protein groups across genetic strains. Therefore, this study developed metrics based on visual parameters of the previously mentioned scatter plot. Metrics calculated from these plots are intuitive, and have easily interpretable biological implications regarding the modulation of these measurements under two experimental conditions. Three metrics were used were used to interpret biological significance: Polygonal Area, Euclidian Distance, and Directional Index. Using the points on an individual plot, a polygon is drawn around the points.

The calculated Polygonal Area represents the two-dimensional turnover range that the specific functional group occupies; this biologically indicates the intrinsic synchronization underlying protein turnover fluctuating between normal and stressed conditions. A smaller polygonal area implies high synchronicity of turnover, and could imply stringent regulatory mechanisms within a genetic strain. A large polygonal area indicates a large turnover range for a group, and can show that there is no direct or less concerted regulatory mechanism applied to individual subunits within the functional group. For each individual protein within a group, the distance from the zero-alteration line was calculated. The absolute values of the distance calculations were averaged; the mean absolute distance serves as a measure of the susceptibility of the protein group towards ISO stimulation. A larger Euclidian Distance illustrates a greater overall turnover variation of a protein group. Finally, for a group of proteins, the number of proteins with increased turnover was compared with the number of proteins with decreased turnover to create the Directional Index. This parameter elucidates the tendency of ISO impact upon protein turnover, and the convergence or divergence of alterations. This index ranges from -1 to 1: a "-1" indicates every protein in a group has decreased turnover, and a "+1" means a functional group is turned over more rapidly. A value close to 0 indicates a divergent trend.

Statistical Analysis

The uniqueness of proteasomal protein turnover was found by applying Student's t-test to proteasomal turnover rates compared to those of other functional clusters (non-proteasomal degradation, ribosomal, and contractile proteins). This was done for both experimental conditions separately. When comparing the metrics across six genetic strains for one protein cluster, one-way ANOVA was applied to the absolute distances for each protein group. If the group had a significant p-value, post-hoc testing was applied. To statistically determine the differences in protein distance among strains, a Wilcoxon-Rank test was applied to each protein group. All of the p-values were then adjusted by applying a Benjamini-Hochberg correction using a false discovery rate of 0.35.

To determine the proteins whose turnover rate was significantly altered between normal and hypertrophied conditions for the proteasomal and contractile clusters, the turnover of a given protein was averaged across all six strains for each experimental condition. From these average values, the fold change was calculated. In addition, a p-value was calculated for every protein when comparing the values for normal and hypertrophied conditions across the six strains; these values are adjusted by applying a Benjamini-Hochberg correction using 0.35 as the false discovery rate for both sets of statistical tests. To the resulting fold change and p-values for each protein, the following thresholds were applied: fold change was greater than 1.2 or less than 0.8, and adjusted Benjamini Hochberg p-value is greater than 0.35. The proteins that fit into that threshold were reported to have differentially altered turnover rates at a statistically significant level. All of these analyses are performed in R.

Results

Temporal Dataset Enables Protein Turnover Quantification for Selected Functional Groups

This entire dataset comprises half-life information for 3230 proteins; of these, 863 were quantified for both control and hypertrophy conditions for all six strains, hereby noted as “complete”. Of the 53 proteasomal proteins in Table 5, 29 had complete measurements. Among the 121 non-proteasomal degradation proteins chosen for this study, 10 were completely characterized for turnover. Identifying synthesis machineries produced similar results; 26 out of 80 were identified entirely. Finally, turnover rate was quantified entirely for 45 of the 60 contractile proteins. This data, along with the quartile ranges for each functional cluster, are listed in Tables 5 and 6.

Protein Turnover Features among Six Genetic Mouse Strains

The six genetic strains profiled in this dataset encompass a wide range of cardiac phenotypes, in that they all display distinct responses to hypertrophic stimulation among proteasomal components (adjusted $p = 0.021$) and contractile proteins (adjusted $p < 0.0001$) Nevertheless, differences in half-life range and modulation should be noted as a qualitative assessment of the sample population. The metrics used in this comparison are Polygonal Area (A), Euclidian Distance (D), and Directional Index (I); these results are summarized in Table 7.

Proteasomal machineries exhibit the lowest average distance metric of any of the four functional groups; when comparing strains, Distance is statistically highest for C57BL/6J (D: 1.09 | A: 65.45) and DBA/2J (D: 0.95 | A: 69.18), though their Directional Indices vary, in that I for C57BL/6J (-0.3) is less polar than that of DBA/2J (-0.8). The CE/J proteasomal subunits are statistically lower than C57BL/6J regarding Distance at 0.43, with Area following a similar trend at 16.33. BALBc/J and FVB/NJ have moderate, statistically indistinguishable Distance metrics (0.59 and 0.80), with both sets having a positive Index. These characteristics are all distinct from those of the non-proteasomal degradation machineries. Within the non-proteasomal

protein group, there are biological classes that have unique mechanisms: lysosomal proteins display a small range of protein turnover and little change, while protease enzyme proteins lie in a larger range and experience greater difference in turnover rate. Ribosomal proteins, in contrast, display higher Area (average A: 94.72) and the largest average Distance of any protein group; the group as a whole displays a decreased trend (D: 1.46, $p = 0.014$ | I: -0.6). Contractile proteins display a fairly broad range of turnover, with a Polygonal Area of 95.68 averaged across all six strains. These proteins also exhibit a fairly low, statistically indistinguishable average Distance (0.83), regardless of strain. A six-strain comparison revealed that CE/J (D: 0.870), DBA/2J (1.025), and BALBc/J (0.872) experienced the statistically highest level of contractile turnover adjustment ($p = 0.034$), despite having lower two-dimensional Area metrics than other strains with lowered levels of modification.

When examining individual strains across all protein groups, it is apparent that A/J and DBA/2J demonstrate the largest half-life alteration, as well as the largest directional trends, while the other strains have Distance metrics in a close range. FVB/NJ and BALBc/J have non-negative Directional Indices (0.2 and 0.0, respectively), which contrasts highly with the negative Indices of the other four strains.

Proteasomal Components Exhibit Distinct Self-regulatory Mechanisms Among Total Proteins, Degradation and Synthesis Machineries

The half-lives for proteasome subunits, non-proteasomal degradation proteins, and ribosome subunits were visualized for each genetic strain in Figure 1. Proteasome turnover ranges under both control and hypertrophy conditions displayed narrow ranges of turnover. Interquartile ranges for proteasomal machinery half-life was 3.58-5.45 days in control and 3.51-5.23 days for ISO conditions. This is significantly different from that of the entire proteome (IQR control: 3.95-11.56 d, $p < 0.0001$ | hypertrophy: 3.56-11.21 d, $p < 0.0001$). The turnover dynamics of other key degradation components, including the autophagy-lysosome system and singular proteases, span a much broader range under both conditions, and are statistically

different from those of the proteasome (IQR control: 2.10-9.32 d, p = 0.004 | hypertrophy: 2.48-9.35 d, p = 0.0008). Selected synthesis machineries (i.e., the ribosome) span a narrower interquartile range than that of the proteasome, but contain more proteins with outlying turnover rates. Specifically, interquartile ranges for ribosomal machinery half-life was 6.68-8.86 days in control and 5.42-7.07 days for ISO conditions; the proteasomal turnover machineries are also statistically different from this population (p-value for both < 0.0001).

Proteasomal Turnover Rate Variation Differs by Individual Subunit

Following β-adrenergic stimulation via ISO, two proteasomal proteins were identified as having a significantly modulated protein turnover between control and experimental conditions at a Benjamini-Hochberg corrected p-value < 0.4. Proteasome subunit alpha type-5 (PSMA 5), a core alpha subunit protein within the 20S proteasome, had a fold-change value of 0.86, meaning the half-life of the protein decreased under hypertrophic conditions. Heat shock protein HSP 90-beta (HSP90AB1), a member of a group of chaperone proteins that can act as a mediator during misfolded or damaged protein degradation as well as during translation of proteins, was also identified, having a fold change value of 1.60, denoting an increased half-life under hypertrophic conditions. These proteins and comparisons are highlighted in Figure 2 and Table 8A.

Comparison of Proteasomal Turnover Rate Among Other Datasets Involving Diverse Tissues and Model Systems

Proteasomal subunit turnover rates were extracted from literature for different tissues (liver, muscle, kidney, brain)[34] and model systems (bank vole).[2] The turnover rates produced by this dataset closely follow the turnover rates discovered in previous mouse heart datasets for other genetic strains (Control: 4.4-7.3 days | ISO: 3.8-7.2 days).[16] In addition, these data follow trends seen in other tissue types, in that the range of heart proteasome subunit half-lives is comparable to that of skeletal muscle (12.4-15.7 | 8.8-22.3),[2] and brain tissue (Control: 4.9-

5.3),[34] but much higher than the range of liver proteasomal subunits (Bank Vole: 0.9-7.6 | 2.3-15.3).[2]

Identification of Contractile Proteins Most Sensitive to Hypertrophic Stimulation

Through applying statistical and differential thresholds, a total of ten contractile proteins were found to be significantly differentially expressed across all six strains. Among cardiac thick filament protein components, the ventricular isoform of myosin essential light chain (MYL3) and the cardiac isoform of α-myosin heavy chain (MYH6) were differentially modified; among thin filament proteins, the cardiac isoforms of troponin I (TNNI3) and troponin C (TNNC1) were identified. Among other structural classifications as the intercalated disks, obscurin (OBSCN), cypher (LDB3), α-II spectrin (SPTAN1), n-cadherin (CDH2), desmoglein-2 (DSG2), and the cardiac isoform of α-actinin (ACTN2) were identified among all six strains. These results are summarized in Figure 3 and Table 8B.

Discussion

Half-life profiling of functional groups across six strains yielded unique insights into the strain-specific adaptive behavior proteins under cardiac stress. Proteasomal subunit turnover is less altered than that of other functional groups, implying distinctive regulatory mechanisms. Specifically among the six strains, ISO induces greater turnover modification in C57BL/6J and DBA2J mice, with C57BL/6J having a divergent response and DBA2J exhibiting concerted decreased turnover. Turnover of CE/J proteasomal subunits are the most resilient to ISO-induced stress, and exhibit the highest synchronicity. Proteasome subunits in BALBc/J and FVB/NJ are moderately responsive to ISO; DBA exhibits concerted increased turnover, while BALBc/J has a divergent response. Across all six strains, contractile proteins exhibit a larger range in both experimental and ISO conditions, with change in turnover rates. Strains whose contractile units are most susceptible are CE/J, DBA/2J, and BALBc/J; ISO enhances turnover rate in BALBc/J, and decreases turnover in CE/J and DBA/2J. A/J contractile proteins are resilient in response to ISO-induced stress, primarily exhibiting slower turnover among subunits. Finally, C57BL/6J and FVB/NJ exhibit resilient, divergent ISO-induced turnover modulation.

In inspecting four different functional groups – proteasome components, non-proteasome degradation factors, ribosome complexes, and contractile proteins – there are patterns underlying protein turnover signatures for individual strains. The strains most sensitive to ISO stimulation are DBA/2J and A/J; the proteins profiled in these strains primarily experience reduced turnover rates. This information aligns with previously reported phenotypic characteristics of these two strains in response to hypertrophy, in that both DBA/2J and A/J are particularly sensitive to hypertrophic stimulation.[35] FVB/NJ and BALBc/J are the most resilient across the board; interestingly, in contrast to the rest of the strains, FVB/NJ and BALBc/J proteins tend to turn over faster in ISO-induced hypertrophy. Between the two strains with an overall moderate response to hypertrophy, CE/J and C57BL/6J, there exist noticeable patterns. For example, C57BL/6J has heightened turnover modulation of proteasomal subunits, but less

alteration of contractile protein turnover rates; this might imply distinct downstream effects of the proteasome within this strain. Moreover, CE/J proteasomal subunits were the least sensitive to induced hypertrophy, but exhibited a higher rate of contractile turnover alteration. Taken together, these characteristics define these six strains as phenotypically distinct, and can encapsulate some of the changes seen in a genetically diverse population.

Two proteasomal constituents were identified to be significantly altered in hypertrophy in this study; both of which have been studied in many other disease model systems. PSMA5, a portion of the 20S catalytic particle, displayed increased half-life under ISO stimulation, implying a slower incorporation of $^{2}H_2O$, and slower rate of synthesis. PSMA5, also termed α5, is responsible for the first step of proteasome complex assembly and formation of the mature α-ring; indeed, α5 serves as the binding site for chaperones,[36 37] and is susceptible to many post-translational modifications.[38 39] The α5 subunit displays endoribonuclease activity, and is able to degrade the mRNA of regulatory transcription factor genes such as c-myc and c-fos.[40] The data presented here aligns with the findings from gene and mRNA transcript expression studies involving many organ systems and disease types.[41 42 43 44] Notably, in a study involving high fat diet-induced obesity in two mouse strains, C57BL/6J and BALB/c, PSMA5 was transcriptionally up-regulated in C57BL/6J mice and down-regulated in BALB/c mice, which may imply differential susceptibilities and therefore responses to cellular insult.[45] Taken together, these studies and the findings presented here illustrate PSMA5 as a sensitive indicator of overall proteasome function across multiple dimensions of molecular profiles.

The other identified protein is Heat shock protein 90-beta (HSP90AB1), which had a decreased half-life and therefore increased rate of protein turnover in hypertrophy. As a chaperone protein and reported associating partner for proteasomal complex, HSP90AB1 binds and stabilizes other proteins by utilizing ATP.[46] If a protein is improperly folded, HSP90AB1 can initiate and catalyze protein degradation.[47] This protein is part of a family whose gene expression is increased in cancer cells; they are thought to stabilize mutant proteins that allow

for the malignancy of tumor proliferation. As such, they have been targeted for cancer treatment in salivary gland, pulmonary, and other specific tumor types.[48] [49] [50] In a cardiac murine model, HSP90AB1 has been found to bind extracellularly to TGFβ receptor I, and induce the TGFβ-mediated collagen synthesis in fibroblasts found in the heart.[51] In other mammalian models, increased expression of the protein HSP90AB1 during hibernation cycles has cardio-protective effects during induced ischemia-reperfusion injury.[52]

In addition, ten contractile proteins are significantly differentially altered during cardiac stress; these ten proteins could serve as markers for pathological changes in the cardiac phenotype under β-adrenergic stimulation. The functional categories identified span many physical aspects of the sarcomere, including the Z-line (OBSCN, ACTN2, and LDB3), desmosomes (DSG2), adherens junctions (CDH2), and intercalated disks (SPTAN1). The targets represent proteins that can be assessed for post-translational modifications involved in protein turnover, such as protein ubiquitination; the modifications of these targets can provide unique insights as to the manifestation of previously observed physiological phenomena, such as enhanced contractile force.[53]

The information elucidated from this study should be taken with a few considerations, as there were necessary assumptions made in both dataset generation and analysis of extracted functional groups. Two animals were used per strain and per time point, which limits the statistical power of the dataset, and confines the potential analyses. In addition, the turnover rate was calculated as an average of both biological samples per time point, rather than individually; as the biological samples should have little genetic variance, it is not likely this could lead to confounding factors, but should be noted nonetheless. Moreover, every mouse profiled in this study was male, which does not necessarily illustrate the effects of hypertrophy in an unbiased, sex-neutral fashion. Further studies with tailored experimental design will need to be performed to determine sex differences, if any. Finally, profiled mice were in an adolescent life stage, meaning that their hearts and bodies were still growing at the time of profiling.

In addition, assumptions were made within the ProTurn software regarding statistical modeling and determination of the protein turnover rate. To assess the rate of $^{2}H_2O$ incorporation into newly synthesized proteins, the creators of ProTurn make the assumption that the protein expression levels eventually reach steady-state, though the time taken to reach steady-state is assessed individually. The authors point out that this initial modeling is not accurate for proteins that have slow turnover rates or large half-lives, and that additional modifications to the algorithm were made to account for these specimens. When examining the dataset, this can be seen in the MAD value for each measurement, which denotes the possible error. They also point out that a turnover rate, including error, could not be calculated for every experimental condition and mouse strain. Indeed, only 823 proteins had data for all experimental factors. Finally, the current method did not differentiate isoforms within a protein pool, including immature protein precursor, matured protein, damaged protein, or any different post-translational modifications.

In the analysis of the selected functional clusters, a few factors are worth consideration. The metrics used here are somewhat sensitive to outliers, particularly the Area metric. A potential solution is to use a density or other model to determine extensive outliers, and exclude the data. Finally, one assumption made to compare statistical significance of individual proteins was that an average of the turnover rate across the strains for a particular protein encapsulates the biological phenomena. However, each of the strains has a different genetic makeup, and therefore will experience different physiological responses to isoproterenol stimulation. Additionally, a fold-change threshold of 20% was applied to reveal differentially altered protein half-lives; as half-lives already encompass the rate of protein synthesis and degradation, changes greater than 20% are considered biologically relevant.

The findings of this study can be used for translational applications. The two identified protein targets, PSMA5 and HSP90AB1, can be quantified for temporal protein and gene expression in response to isoproterenol, which would confirm their roles in hypertrophy-induced

molecular pathways. Upon confirmation, targeted approaches can be used to determine how regulating specific proteasomal subunit activity can affect contractile targets. For example, assessing the post-translational modifications of these proteins, as well as subcellular localization, can determine how these proteins are regulated. Additionally, small molecules that mediate turnover of PSMA5 and HSP90AB1 can be used in a dose-dependent fashion, and contractile targets can be assessed to determine the role of these proteasomal subunits in mediating hypertrophic effects.

On a larger scale, there are biological experiments that can be used to further elucidate the heterogeneous turnover behaviors of targeted functional groups among these 6 genetic mouse strains. In basal conditions, the net proteolytic activity of a myocardial proteome is supported by the subpopulation of mature and functionally active proteasomal complexes, which is determined by both expressional level of proteasomal components and their basal turnover rate. To paint a more comprehensive picture, more parameters are needed to define the system. The basal expression of proteasomal components for 6 genetic strains needs to be seen in combination with this turnover comparison; doing so can identify the intrinsic proteasomal capacity. Under ISO treatment, the proteolytic activities for these mouse strains can be assessed and compared with basal conditions to ascertain phenotypic manifestations of ISO stimulation. Within the proteasome, examining the differences in complex assembly may determine the effects of cellular insult on the creation of functionally mature complexes.

Although other key degradation proteins were not the focus of this study, this analysis yielded interesting observations. Hypertrophic stimulation underscored the intrinsic regulation of the identified lysosomal proteins, which greatly contrasted with protease enzyme modulation. There are many potential explanations for this phenomenon that may include modulation of mitochondrial enzymes as a result of changing energetic demands on the cell. As such, measuring proteolytic activities of these degradation proteins will determine the distinctive

nature of proteasomal turnover regulation, and provide a more holistic understanding of protein degradation within the cell.

This large, unbiased dataset has wide applicability and utility, and provides a wealth of information. The creators of this dataset highlight multiple use cases for specific aspects of biology, and there are further analyses that can be performed specific to proteasomes and other machineries underlying protein turnover regulation. As previously stated, this study took averages of turnover rates across six strains, ignoring genetic differences that may underlie hypertrophied conditions. Once a protein signature of cardiac cell growth has been established for each strain, the effects of differential susceptibility on protein turnover rates can be correlated, and the strains can be stratified using a combination of both statistical and machine learning methods. Specifically, the changes occurring at a protein level can be associated with changes in phenotypic markers of hypertrophic manifestations, such as the heart weight/body weight. On a larger scale, this data can be integrated with steady-state proteomics data to provide a fuller illustration of the complex interplay between protein expression and turnover. This dataset also includes label-free protein expression distribution data at aforementioned time points in the form of normalized spectral abundance factor (NSAF) values.[31] For greater temporal resolution, a proteomics expression method involving labels, such as Tandem Mass Tags (TMT), could be employed to thoroughly and accurately assess protein turnover.[54] Finally, in parallel, there is potential to explore the genetic regulation of protein turnover by exploring genetic mapping strategies, particularly by looking into SNPs for each genetic strain.

Proteasomal subunit structure and function have been studied in a myriad of disease states; a compromised complex assembly or a dysfunctional proteasome function can serve as potential drug targets. Reduced proteolytic activities and diminished protein quality control drive pathological phenotypes found in neurodegenerative diseases,[55] [56] [57] adverse immunological responses,[58] the malignant transformation of cell growth,[59] and cardiovascular diseases.[60] [61] Specifically, the proteasome plays a significant role in ischemic injury,[62] heart failure,[63] and

hypertrophy.[64] This study identifies two individual proteasomal subunits that are most sensitive to ISO; in addition, contractile proteins with high levels of susceptibility create a molecular pattern of phenotypic cardiac response to β-adrenergic stimulation.

Complex interactions of genes, transcripts, proteins, and small molecules underlie phenotypic manifestations in response to stressors. Varying degrees of biological resilience within and among systems necessitate investigations that employ multiple dimensions of data. In the burgeoning era of integrative omics, research is trending toward using multiple parameters to define a biological system, so as to better understand these interactions. As a more comprehensive understanding of protein turnover is developed, we are learning more the regulation of protein function as it pertains to cardiac diseases. Moving forward, there is a need for functional analysis to stratify populations within a protein species pool and assign functions to them. With characterization, quantification, and functional data, there exist multiple dimensions of information to decode the molecular foundation of proteome dynamics during cardiac stress.

Figure 1: Half-Life Alteration of Protein Degradation and Synthesis Machineries in ISO-stressed Murine Cardiomyocytes

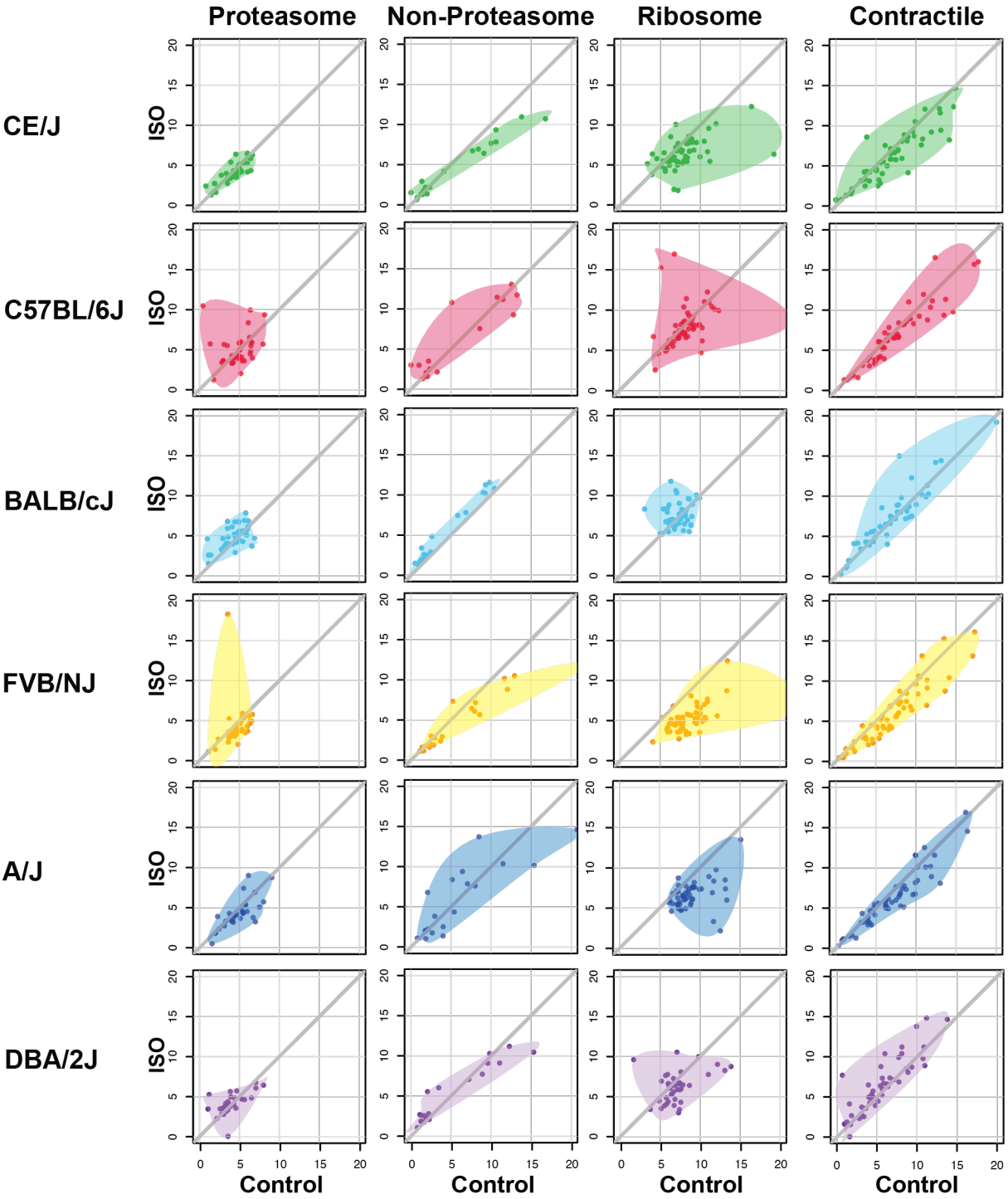

Figure 1: Global Assessment of proteasome machineries in the context of other protein turnover machineries and contractile proteins. Scatter plot denoting the turnover perturbation under control and hypertrophic conditions. X-axis value: turnover in control condition, Y-axis value: turnover in ISO conditions. Gray line: zero perturbation line. Polygon drawn around points includes error. Larger versions of these plots are available in a published R Markdown file.

Figure 2: Assessment of Proteasome Machineries Across Six Genetic Strains

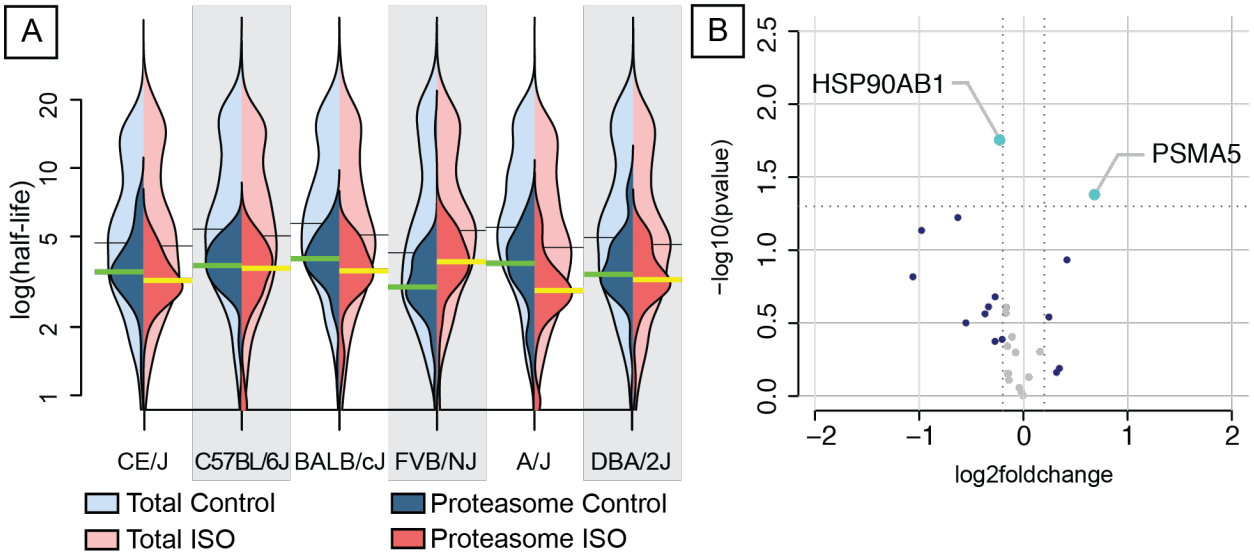

Figure 2: Comparison of proteasomal machineries across genetic strains and identification of significantly altered protein half-lives. **(A)** Violin plots detailing the distribution of proteasomal subunit turnover. Plots are overlain violin plots of the total protein pool for clarity. All violin plots are based on density. Green line: median half-life in control. Yellow line: median half-life in ISO condition. **(B)** Volcano plot identifying significant protein turnover perturbation. Two proteins were identified through a statistical threshold: $p<0.05$ and differential threshold: 20% fold change.

Figure 3: Assessment of Contractile Machineries Across Six Genetic Strains

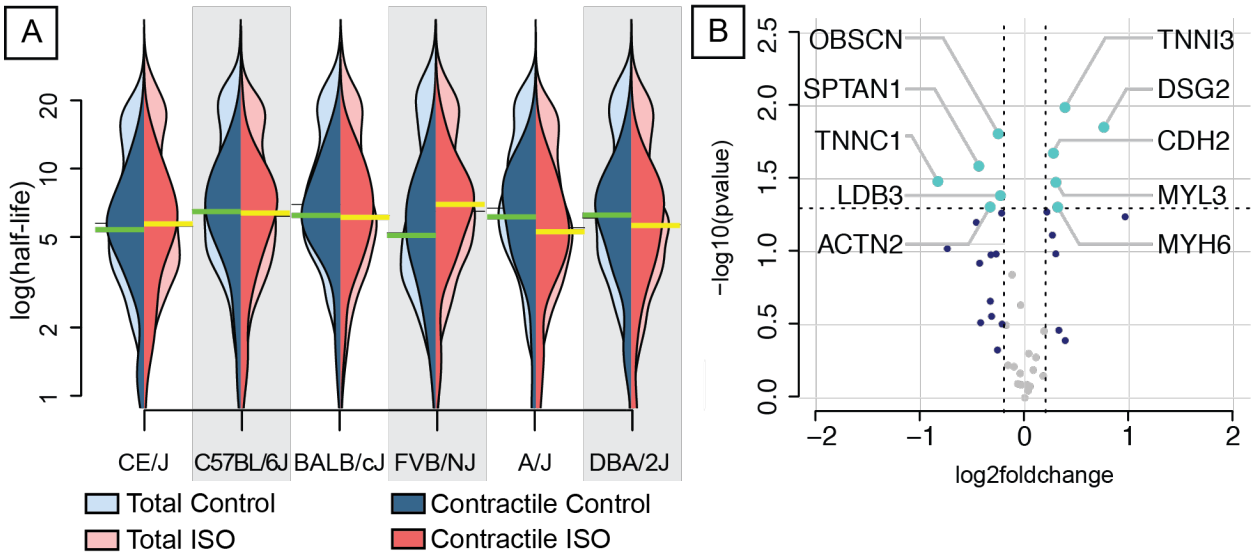

Figure 3: Comparison of contractile proteins across genetic strains and identification of significantly altered protein half-lives. **(A)** Violin plots detailing the distribution of protein subunit half-life. Plots are overlain violin plots of the total protein pool for clarity. All violin plots are based on density. Green line: median half-life in control. Yellow line: median half-life in ISO condition. **(B)** Volcano plot identifying significant protein turnover perturbation. Ten proteins are identified through these means. Statistical threshold: $p<0.05$, differential threshold: 20% fold change.

Table 1: Proteasomal Protein List

Gene Name	Protein Name	UniProt ID
PSMA1	Proteasome subunit alpha type-1	**Q9R1P4**
PSMA2	Proteasome subunit alpha type-2	**P49722**
PSMA3	Proteasome subunit alpha type-3	**O70435**
PSMA4	Proteasome subunit alpha type-4	**Q9R1P0**
PSMA5	Proteasome subunit alpha type-5	**Q9Z2U1**
PSMA6	Proteasome subunit alpha type-6	**Q9QUM9**
PSMA7	Proteasome subunit alpha type-7	**Q9Z2U0**
PSMB1	Proteasome subunit beta type-1	**O09061**
PSMB2	Proteasome subunit beta type-2	**Q9R1P3**
PSMB3	Proteasome subunit beta type-3	**Q9R1P1**
PSMB4	Proteasome subunit beta type-4	**P99026**
PSMB5	Proteasome subunit beta type-5	**O55234**
PSMB6	Proteasome subunit beta type-6	**Q60692**
PSMB7	Proteasome subunit beta type-7	**P70195**
PSMB8	Proteasome subunit beta type-8	**P28063**
PSMB9	Proteasome subunit beta type-9	**P28076**
PSMB10	Proteasome subunit beta type-10	**O35955**
PSMC1	26S protease regulatory subunit 4	**P62192**
PSMC2	26S protease regulatory subunit 7	**P46471**
PSMC3	26S protease regulatory subunit 6A	**O88685**
PSMC4	26S protease regulatory subunit 6B	**P54775**
PSMC5	26S protease regulatory subunit 8	**P62196**
PSMC6	26S protease regulatory subunit 10B	**P62334**
PSMD1	26S proteasome non-ATPase regulatory subunit 1	**Q3TXS7**
PSMD2	26S proteasome non-ATPase regulatory subunit 2	**Q8VDM4**
PSMD3	26S proteasome non-ATPase regulatory subunit 3	**P14685**
PSMD4	26S proteasome non-ATPase regulatory subunit 4	**O35226**
PSMD5	26S proteasome non-ATPase regulatory subunit 5	**Q8BJY1**
PSMD6	26S proteasome non-ATPase regulatory subunit 6	**Q99JI4**
PSMD7	26S proteasome non-ATPase regulatory subunit 7	**P26516**
PSMD8	26S proteasome non-ATPase regulatory subunit 8	**Q9CX56**
PSMD9	26S proteasome non-ATPase regulatory subunit 9	**Q9CR00**
PSMD10	26S proteasome non-ATPase regulatory subunit 10	**Q9Z2X2**
PSMD11	26S proteasome non-ATPase regulatory subunit 11	**Q8BG32**
PSMD12	26S proteasome non-ATPase regulatory subunit 12	**Q9D8W5**
PSMD13	26S proteasome non-ATPase regulatory subunit 13	**Q9WVJ2**
PSMD14	26S proteasome non-ATPase regulatory subunit 14	**O35593**
ADRM1	Proteasomal ubiquitin receptor ADRM1	**Q9JKV1**
SHFM1	26S proteasome complex subunit DSS1	**P60897**
PSME1	Proteasome activator complex subunit 1	**P97371**

PSME2	Proteasome activator complex subunit 2	**P97372**
PSME3	Proteasome activator complex subunit 3	**P61290**
PSME4	Proteasome activator complex subunit 4	**Q5SSW2**
POMP	Proteasome maturation protein	**Q9CQT5**
PSMG1	Proteasome assembly chaperone 1	**Q9JK23**
PSMG2	Proteasome assembly chaperone 2	**Q9EST4**
PSMG3	Proteasome assembly chaperone 3	**Q9CZH3**
PSMG4	Proteasome assembly chaperone 4	**P0C7N9**
PSME4	Proteasome activator complex subunit 4	**Q5SSW2**
HSP90AA1	Heat shock protein HSP 90-alpha	**P07901**
HSP90AB1	Heat shock protein HSP 90-beta	**P11499**
ECM29	Proteasome-associated protein ECM29 homolog	**Q6PDI5**
BAG6	Large proline-rich protein BAG6	**Q9Z1R2**

Table 2: Non-proteasomal Degradation Protein List

Gene Name	Protein Name	UniProt ID
GAA	Lysosomal alpha-glucosidase	**P70699**
IFI30	Gamma-interferon-inducible lysosomal thiol reductase	**Q9ESY9**
MAN2B1	Lysosomal alpha-mannosidase	**O09159**
ACP5	Tartrate-resistant acid phosphatase type 5	**Q05117**
ACP2	Lysosomal acid phosphatase	**P24638**
PRCP	Lysosomal Pro-X carboxypeptidase	**Q7TMR0**
GALNS	N-acetylgalactosamine-6-sulfatase	**Q571E4**
PPT2	Lysosomal thioesterase PPT2	**O35448**
NAGA	Alpha-N-acetylgalactosaminidase	**Q9QWR8**
GNS	N-acetylglucosamine-6-sulfatase	**Q8BFR4**
AGA	N(4)-(beta-N-acetylglucosaminyl)-L-asparaginase	**Q64191**
ASAH1	Acid ceramidase	**Q9WV54**
LIPA	Lysosomal acid lipase/cholesteryl ester hydrolase	**Q9Z0M5**
IL4I1	L-amino-acid oxidase	**O09046**
ARSA	Arylsulfatase A	**P50428**
ARSB	Arylsulfatase B	**P50429**
ARSG	Arylsulfatase G	**Q3TYD4**
CTSB	Cathepsin B	**P10605**
CTSD	Cathepsin D	**P18242**
CTSF	Cathepsin F	**Q9R013**
CTSH	Pro-cathepsin H	**P49935**
CTSK	Cathepsin K	**P55097**
CTSL	Cathepsin L1	**P06797**
CTSO	Cathepsin O	**Q8BM88**
CTSS	Cathepsin S	**O70370**
CTSZ	Cathepsin Z	**Q9WUU7**
CLN5	Ceroid-lipofuscinosis neuronal protein 5 homolog	**Q3UMW8**
CREG1	Protein CREG1	**O88668**
DNASE2	Deoxyribonuclease-2-alpha	**P56542**
CTBS	Di-N-acetylchitobiase	**Q8R242**
CTSC	Dipeptidyl peptidase 1	**P97821**
FUCA1	Tissue alpha-L-fucosidase	**Q99LJ1**
GALC	Galactocerebrosidase	**P54818**
GLA	Alpha-galactosidase A	**P51569**
GLB1	Beta-galactosidase	**P23780**
GM2A	Ganglioside GM2 activator	**Q60648**
GBA	Glucosylceramidase	**P17439**
GUSB	Beta-glucuronidase	**P12265**
GGH	Gamma-glutamyl hydrolase	**Q9Z0L8**
HEXA	Beta-hexosaminidase subunit alpha	**P29416**

HEXB	Beta-hexosaminidase subunit beta	**P20060**
HYAL1	Hyaluronidase-1	**Q91ZJ9**
IDS	Iduronate 2-sulfatase	**Q08890**
IDUA	Alpha-L-iduronidase	**P48441**
LGMN	Legumain	**O89017**
EPDR1	Mammalian ependymin-related protein 1	**Q99M71**
MANBA	Beta-mannosidase	**Q8K2I4**
MPO	Myeloperoxidase	**P11247**
NPC2	Epididymal secretory protein E1	**Q9Z0J0**
PPT1	Palmitoyl-protein thioesterase 1	**O88531**
PLA2G15	Group XV phospholipase A2	**Q8VEB4**
PLBD2	Putative phospholipase B-like 2	**Q3TCN2**
CTSA	Lysosomal protective protein	**P16675**
RNASET2	Ribonuclease T2	**Q9CQ01**
PSAP	Prosaposin	**Q61207**
SCPEP1	Retinoid-inducible serine carboxypeptidase	**Q920A5**
SIAE	Sialate O-acetylesterase	**P70665**
NEU1	Sialidase-1	**O35657**
NEU4	Sialidase-4	**Q8BZL1**
SMPD1	Sphingomyelin phosphodiesterase	**Q04519**
TPP1	Tripeptidyl-peptidase 1	**O89023**
LAMP1	Lysosome-associated membrane glycoprotein 1	**P11438**
LAMP2	Lysosome-associated membrane glycoprotein 2	**P17047**
LAMP3	Lysosome-associated membrane glycoprotein 3	**Q7TST5**
LAMP5	Lysosome-associated membrane glycoprotein 5	**Q9D387**
SCARB2	Lysosome membrane protein 2	**O35114**
CD63	CD63 antigen	**P41731**
CTNS	Cystinosin	**P57757**
SLC17A5	Sialin	**Q8BN82**
CLCN7	H(+)/Cl(-) exchange transporter 7	**O70496**
OSTM1	Osteopetrosis-associated transmembrane protein 1	**Q8BGT0**
ATP13A2	Probable cation-transporting ATPase 13A2	**Q9CTG6**
MCOLN1	Mucolipin-1	**Q99J21**
MCOLN2	Mucolipin-2	**Q8K595**
MCOLN3	Mucolipin-3	**Q8R4F0**
SLC15A3	Solute carrier family 15 member 3	**Q8BPX9**
SLC2A8	Solute carrier family 2, facilitated glucose transporter member 8	**Q9JIF3**
SLC29A3	Equilibrative nucleoside transporter 3	**Q99P65**
SLC11A1	Natural resistance-associated macrophage protein 1	**P41251**
SLC11A2	Natural resistance-associated macrophage protein 2	**P49282**
SLC36A1	Proton-coupled amino acid transporter 1	**Q8K4D3**
SLC30A2	Zinc transporter 2	**Q2HJ10**

ABCA2	ATP-binding cassette sub-family A member 2	**P41234**
ABCA3	ATP-binding cassette sub-family A member 3	**Q8R420**
ABCB9	ATP-binding cassette sub-family B member 9	**Q9JJ59**
LMBRD1	Probable lysosomal cobalamin transporter	**Q8K0B2**
MFSD8	Major facilitator superfamily domain-containing protein 8	**Q8BH31**
SLC26A11	Sodium-independent sulfate anion transporter	**Q80ZD3**
HGSNAT	Heparan-alpha-glucosaminide N-acetyltransferase	**Q3UDW8**
SPPL2A	Signal peptide peptidase-like 2A	**Q9JJF9**
NCSTN	Nicastrin	**P57716**
PSEN1	Presenilin-1	**P49769**
TMEM55A	Type 2 phosphatidylinositol 4,5-bisphosphate 4-phosphatase	**Q9CZX7**
TMEM55B	Type 1 phosphatidylinositol 4,5-bisphosphate 4-phosphatase	**Q3TWL2**
VAMP7	Vesicle-associated membrane protein 7	**P70280**
CLN3	Battenin	**Q61124**
NPC1	Niemann-Pick C1 protein	**O35604**
CYB561A3	Cytochrome b ascorbate-dependent protein 3	**Q6P1H1**
TMEM192	Transmembrane protein 192	**Q9CXT7**
TMEM63A	CSC1-like protein 1	**Q91YT8**
EVA1A	Protein eva-1 homolog A	**Q91WM6**
TMEM74	Transmembrane protein 74	**Q8BQU7**
CD164	Sialomucin core protein 24	**Q9R0L9**
LAPTM4A	Lysosomal-associated transmembrane protein 4A	**Q60961**
LAPTM5	Lysosomal-associated transmembrane protein 5	**Q61168**
TM9SF1	Transmembrane 9 superfamily member 1	**Q9DBU0**
PSME3	Proteasome activator complex subunit 3	**P61290**
LONM	Lon protease homolog, mitochondrial	**Q8CGK3**
CLPX	ATP-dependent Clp protease ATP-binding subunit clpX-like,	**Q9JHS4**
CLPP	ATP-dependent Clp protease proteolytic subunit, mitochondrial	**O88696**
YMEL1	ATP-dependent zinc metalloprotease YME1L1	**O88967**
AFG32	AFG3-like protein 2	**Q8JZQ2**
SPG7	Paraplegin	**Q3ULF4**
OMA1	Metalloendopeptidase OMA1, mitochondrial	**Q9D8H7**
PARL	Presenilins-associated rhomboid-like protein, mitochondrial	**Q5XJY4**
HTRA2	Serine protease HTRA2, mitochondrial	**Q9JIY5**
IMP1L	Mitochondrial inner membrane protease subunit 1	**Q9CQU8**
IMP2L	Mitochondrial inner membrane protease subunit 2	**Q8BPT6**
MPPA	Mitochondrial-processing peptidase subunit alpha	**Q9DC61**
MPPB	Mitochondrial-processing peptidase subunit beta	**Q9CXT8**
PREP	Presequence protease, mitochondrial	**Q8K411**

Table 3: Ribosomal Complex Protein List

Gene Name	Protein Name	UniProt ID
RS3A	40S Ribosomal Protein S3A	**P97351**
RSSA	40S Ribosomal Protein SA	**P14206**
RS3	40S Ribosomal Protein S3	**P62908**
RS9	40S Ribosomal Protein S9	**Q6ZWN5**
RS4X	40S Ribosomal Protein S4, X isoform	**P62702**
RS2	40S Ribosomal Protein S2	**P25444**
RS6	40S Ribosomal Protein S6	**P62754**
RS5	40S Ribosomal Protein S5	**P97461**
RS7	40S Ribosomal Protein S7	**P62082**
RS15A	40S Ribosomal Protein S15a	**P62245**
RS8	40S Ribosomal Protein S8	**P62242**
RS16	40S Ribosomal Protein S16	**P14131**
RS20	40S Ribosomal Protein S20	**P60867**
RS10	40S Ribosomal Protein S10	**P63325**
RS14	40S Ribosomal Protein S14	**P62264**
RS23	40S Ribosomal Protein S23	**P62267**
RS12	40S Ribosomal Protein S12	**P63323**
RS18	40S Ribosomal Protein S18	**P62270**
RS29	40S Ribosomal Protein S29	**P62274**
RS13	40S Ribosomal Protein S13	**P62301**
RS11	40S Ribosomal Protein S11	**P62281**
RS17	40S Ribosomal Protein S17	**P63276**
RS15	40S Ribosomal Protein S15	**P62843**
RS19	40S Ribosomal Protein S19	**Q9CZX8**
RS21	40S Ribosomal Protein S21	**Q9CQR2**
RS24	40S Ribosomal Protein S24	**P62849**
RS25	40S Ribosomal Protein S25	**P62852**
RS26	40S Ribosomal Protein S26	**P62855**
RS27	40S Ribosomal Protein S27	**Q6ZWU9**
RS28	40S Ribosomal Protein S28	**P62858**
RS30	40S Ribosomal Protein S30	**P62862**
RS27A	Ubiquitin-40S Ribosomal Protein S27A	**P62983**
RACK1	Receptor of activated protein C kinase 1	**P68040**
RL10A	60S Ribosomal Protein L10a	**P53026**
RL8	60S Ribosomal Protein L8	**P62918**
RL3	60S Ribosomal Protein L3	**P27659**
RL4	60S Ribosomal Protein L4	**Q9D8E6**
RL11	60S Ribosomal Protein L11	**Q9CXW4**
RL9	60S Ribosomal Protein L9	**P51410**
RL6	60S Ribosomal Protein L6	**P47911**

RL7A	60S Ribosomal Protein L7a	**P12970**
RLA0	60S acidic Ribosomal Protein P0	**P14869**
RL12	60S Ribosomal Protein L12	**P35979**
RL13A	60S Ribosomal Protein L13a	**P19253**

Table 4: Contractile Protein List

Gene Name	Protein Name	UniProt ID
MYH6	Alpha MHC, Cardiac	**Q02566**
MYH7	Beta MHC, Cardiac	**Q91Z83**
MYH7B	Beta MHC, Cardiac	**A2AQP0**
TTN	Titin, Canonical	**A2ASS6**
MYBPC3	Mybpc, Cardiac	**O70468**
MYL3	ELC, Ventricular	**P09542**
MYOM3	Myomesin	**A2ABU4**
MYOM1	Skelemin	**Q62234**
MYL2	RLC, Ventricular	**P51667**
MYL4	ELC, Atrial	**P09541**
MYL7	RLC, Atrial	**Q9QVP4**
ACTC1	Alpha Actin, Cardiac	**P68033**
TPM1	Alpha Tropomyosin	**P58771**
TNNI3	Tni, Cardiac	**P48787**
TNNC1	Tnc, Cardiac And Slow Skeletal	**P19123**
TNNT2	Tnt, Cardiac	**P50752**
TPM2	Beta Tropomyosin	**P58774**
ACTN2	Alpha Actinin, Cardiac And Skeletal	**Q9JI91**
DES	Desmin	**P31001**
LDB3	Cypher, ZASP (Z-Band Alternatively Spliced PDZ-Motif Protein)	**Q9JKS4**
MYOZ2	Myozenin-2, Calsarcin-1	**Q9JJW5**
PLEC	Plectin	**Q9QXS1**
FLNC	Filamin-C, Gamma Filamin	**Q8VHX6**
NEBL	Nebulette	**Q0II04**
OBSCN	Obscurin	**A2AAJ9**
SORBS2	Argbp2, Sorbin And SH3-Domain-Containing Protein	**Q3UTJ2**
SYNPO2	Myopodin, Synaptopodin-2	**Q91YE8**
CAPZB	Capz Beta	**P47757**
CAPZA2	Capz Alpha-2	**P47754**
MYPN	Myopalladin	**Q5DTJ9**
CSRP3	MLP (Muscle LIM Protein), Cysteine And Glycine-Rich Protein 3	**P50462**
NEXN	Nexilin	**Q7TPW1**
TCAP	Telethonin	**O70548**
PDLIM3	(ALP) Alpha Actinin2-Associated LIM Protein, PDZ And LIM	**O70209**
S100A1	S100a1	**P56565**
ANKRD1	CARP (Cardiac Ankyrin Repeat Protein)	**Q9CR42**
MYH10	Non-Muscle Myosin II-B	**Q61879**
MYOT	Myotillin	**Q9JIF9**
ANKRD2	Arpp	**Q9WV06**
DSP	Desmoplakin	**E9Q557**

SPTAN1	Alpha ii Spectrin	**P16546**
VCL	Vinculin	**Q64727**
JUP	Plakoglobin, Gamma-Catenin	**Q02257**
CTNNA1	Alpha E-Catenin	**P26231**

Table 5: Turnover Quantification for Selected Functional Groups

Protein Group	No.	Control		ISO		Total	
		N_{ID}	N_{ID_C}	N_{ID}	N_{ID_C}	N_{ID}	N_{ID_C}
Proteasome	53	50	29	49	37	50	29
Non-proteasomal Degradation	121	37	11	37	12	40	10
Ribosome	80	75	40	74	33	76	26
Contractile	65	59	45	60	52	60	45
Total	3230	2955	992	2996	1172	3230	863

Table 6: Half-life Distribution for Selected Functional Groups

Protein Group	Control Quartile Range (days)					ISO Quartile Range (days)				
	0%	25%	50%	75%	100%	0%	25%	50%	75%	100%
Proteasome	1.08	3.58	4.32	5.45	9.05	0.04	3.51	4.05	5.23	18.30
Non-proteasome	0.01	2.10	5.51	9.32	15.39	1.37	2.48	6.04	9.35	13.72
Ribosome	2.17	6.68	7.62	8.86	13.38	1.95	5.42	6.65	7.71	16.97
Contractile	0.91	4.51	6.69	9.01	20.06	0.04	4.09	6.05	8.45	19.21
Total	0.01	3.95	6.42	11.56	46.13	0.01	3.56	5.85	11.22	42.34

Table 7A: Area Metric Across Six Strains

Strain	Proteasome	Non-proteasome	Ribosome	Contractile	Strain Avg.
CE/J	16.33	37.39	121.50	98.88	68.53
C57BL/6J	65.45	79.86	149.20	101.00	98.88
BALBc/J	28.41	50.23	69.12	94.26	60.51
FVB/NJ	25.88	18.60	35.53	131.60	52.90
A/J	36.77	127.20	77.74	69.31	77.76
DBA/2J	69.18	68.69	115.20	79.00	83.02
Protein Avg.	40.34	63.66	94.72	95.68	

Table 7B: Index and Distance Metrics Across Six Strains

Strain	Proteasome		Non-proteasome		Ribosome		Contractile		Strain Avg.	
	I	D	I	D	I	D	I	D	I	D
CE/J	-0.4	0.43	-0.3	0.95	-0.6	1.34	-0.5	0.87	-0.5	0.90
C57BL/6J	-0.3	1.01	0.1	1.03	-0.4	1.19	-0.6	0.75	-0.4	0.99
BALBc/J	0.2	0.59	0.3	0.78	-0.5	1.24	0.3	0.87	0.0	0.87
FVB/NJ	0.5	0.80	1.0	0.68	0.0	0.94	0.1	0.70	0.2	0.78
A/J	-0.6	0.70	0.1	1.43	-0.8	1.66	-0.4	0.78	-0.6	1.14
DBA/2J	-0.8	0.95	-0.7	1.12	-0.9	2.41	-0.6	1.03	-0.7	1.38
Protein Avg.	-0.2	0.75	0.1	0.99	-0.6	1.46	-0.3	0.83		

Table 8A: Significantly Altered Proteasomal Proteins

Name	Gene Name	UniProt ID	Fold-change	p-value
Heat shock protein HSP 90-beta	HSP90AB1	P11499	0.86	0.018
Proteasome subunit alpha type-5	PSMA5	Q9Z2U1	1.6	0.042

Table 8B: Significantly Altered Contractile Proteins

Name	Gene Name	UniProt ID	Fold-change	p-value
Obscurin	OBSCN	A2AAJ9	0.85	0.016
Desmoglein-2	DSG2	O55111	1.67	0.014
ELC, ventricular	MYL3	P09542	1.22	0.033
N-cadherin	CDH2	P15116	1.21	0.021
α-II spectrin	SPTAN1	P16546	0.74	0.026
TnC, cardiac and slow skeletal	TNNC1	P19123	0.56	0.033
TnI, cardiac	TNNI3	P48787	1.32	0.010
α-MHC, cardiac	MYH6	Q02566	1.25	0.049
α-actinin, cardiac and skeletal	ACTN2	Q9JI91	0.80	0.049
Cypher, ZASP	LDB3	Q9JKS4	0.86	0.042

References

1. Rosamond W, Flegal K, Furie K, Go A, Greenlund K, Haase N, Hailpern SM, Ho M, Howard V, Kissela B, Kittner S, Lloyd-Jones D, McDermott M, Meigs J, Moy C, Nichol G, O'Donnell C, Roger V, Sorlie P, Steinberger J, Thom T, Wilson M, Hong Y, American Heart Association Statistics C and Stroke Statistics S. Heart disease and stroke statistics--2008 update: a report from the American Heart Association Statistics Committee and Stroke Statistics Subcommittee. *Circulation*. 2008;117:e25-146.
2. Hammond DE, Claydon AJ, Simpson DM, Edward D, Stockley P, Hurst JL and Beynon RJ. Proteome Dynamics: Tissue Variation in the Kinetics of Proteostasis in Intact Animals. *Mol Cell Proteomics*. 2016;15:1204-19.
3. Tardiff JC. Cardiac hypertrophy: stressing out the heart. *J Clin Invest*. 2006;116:1467-70.
4. Xu T, Tang H, Zhang B, Cai C, Liu X, Han Q and Zou L. Exercise preconditioning attenuates pressure overload-induced pathological cardiac hypertrophy. *Int J Clin Exp Pathol*. 2015;8:530-40.
5. Tham YK, Bernardo BC, Ooi JY, Weeks KL and McMullen JR. Pathophysiology of cardiac hypertrophy and heart failure: signaling pathways and novel therapeutic targets. *Arch Toxicol*. 2015;89:1401-38.
6. Weiner RB and Baggish AL. Exercise-induced cardiac remodeling. *Prog Cardiovasc Dis*. 2012;54:380-6.
7. Samak M, Fatullayev J, Sabashnikov A, Zeriouh M, Schmack B, Farag M, Popov AF, Dohmen PM, Choi YH, Wahlers T and Weymann A. Cardiac Hypertrophy: An Introduction to Molecular and Cellular Basis. *Med Sci Monit Basic Res*. 2016;22:75-9.
8. Nichtova Z, Novotova M, Kralova E and Stankovicova T. Morphological and functional characteristics of models of experimental myocardial injury induced by isoproterenol. *Gen Physiol Biophys*. 2012;31:141-51.

9. Petriz BA and Franco OL. Effects of hypertension and exercise on cardiac proteome remodelling. *Biomed Res Int*. 2014;2014:634132.
10. Beroud C, Letovsky SI, Braastad CD, Caputo SM, Beaudoux O, Bignon YJ, Bressac-De Paillerets B, Bronner M, Buell CM, Collod-Beroud G, Coulet F, Derive N, Divincenzo C, Elzinga CD, Garrec C, Houdayer C, Karbassi I, Lizard S, Love A, Muller D, Nagan N, Nery CR, Rai G, Revillion F, Salgado D, Sevenet N, Sinilnikova O, Sobol H, Stoppa-Lyonnet D, Toulas C, Trautman E, Vaur D, Vilquin P, Weymouth KS, Willis A, Laboratory Corporation of America Variant Classification G, Quest Diagnostics Variant Classification G, Network UGGBL, Eisenberg M and Strom CM. BRCA Share: A Collection of Clinical BRCA Gene Variants. *Hum Mutat*. 2016;37:1318-1328.
11. Giri M, Zhang M and Lu Y. Genes associated with Alzheimer's disease: an overview and current status. *Clin Interv Aging*. 2016;11:665-81.
12. Lin E and Lane HY. Machine learning and systems genomics approaches for multi-omics data. *Biomark Res*. 2017;5:2.
13. Cohen FE and Kelly JW. Therapeutic approaches to protein-misfolding diseases. *Nature*. 2003;426:905-9.
14. Balch WE, Morimoto RI, Dillin A and Kelly JW. Adapting proteostasis for disease intervention. *Science*. 2008;319:916-9.
15. Dasuri K, Zhang L and Keller JN. Oxidative stress, neurodegeneration, and the balance of protein degradation and protein synthesis. *Free Radic Biol Med*. 2013;62:170-85.
16. Lam MP, Wang D, Lau E, Liem DA, Kim AK, Ng DC, Liang X, Bleakley BJ, Liu C, Tabaraki JD, Cadeiras M, Wang Y, Deng MC and Ping P. Protein kinetic signatures of the remodeling heart following isoproterenol stimulation. *J Clin Invest*. 2014;124:1734-44.
17. Chen X, Wei S, Ji Y, Guo X and Yang F. Quantitative proteomics using SILAC: Principles, applications, and developments. *Proteomics*. 2015;15:3175-92.

18. Taubert M, Jehmlich N, Vogt C, Richnow HH, Schmidt F, von Bergen M and Seifert J. Time resolved protein-based stable isotope probing (Protein-SIP) analysis allows quantification of induced proteins in substrate shift experiments. *Proteomics*. 2011;11:2265-74.
19. Wang D, Liem DA, Lau E, Ng DC, Bleakley BJ, Cadeiras M, Deng MC, Lam MP and Ping P. Characterization of human plasma proteome dynamics using deuterium oxide. *Proteomics Clin Appl*. 2014;8:610-9.
20. Kim TY, Wang D, Kim AK, Lau E, Lin AJ, Liem DA, Zhang J, Zong NC, Lam MP and Ping P. Metabolic labeling reveals proteome dynamics of mouse mitochondria. *Mol Cell Proteomics*. 2012;11:1586-94.
21. Chan XC, Black CM, Lin AJ, Ping P and Lau E. Mitochondrial protein turnover: methods to measure turnover rates on a large scale. *J Mol Cell Cardiol*. 2015;78:54-61.
22. Lyon RC, Lange S and Sheikh F. Breaking down protein degradation mechanisms in cardiac muscle. *Trends Mol Med*. 2013;19:239-49.
23. Nowis D, Maczewski M, Mackiewicz U, Kujawa M, Ratajska A, Wieckowski MR, Wilczynski GM, Malinowska M, Bil J, Salwa P, Bugajski M, Wojcik C, Sinski M, Abramczyk P, Winiarska M, Dabrowska-Iwanicka A, Duszynski J, Jakobisiak M and Golab J. Cardiotoxicity of the anticancer therapeutic agent bortezomib. *Am J Pathol*. 2010;176:2658-68.
24. Drews O and Taegtmeyer H. Targeting the ubiquitin-proteasome system in heart disease: the basis for new therapeutic strategies. *Antioxid Redox Signal*. 2014;21:2322-43.
25. Smith DM, Chang SC, Park S, Finley D, Cheng Y and Goldberg AL. Docking of the proteasomal ATPases' carboxyl termini in the 20S proteasome's alpha ring opens the gate for substrate entry. *Mol Cell*. 2007;27:731-44.
26. Wang J and Maldonado MA. The ubiquitin-proteasome system and its role in inflammatory and autoimmune diseases. *Cell Mol Immunol*. 2006;3:255-61.
27. Rabl J, Smith DM, Yu Y, Chang SC, Goldberg AL and Cheng Y. Mechanism of gate opening in the 20S proteasome by the proteasomal ATPases. *Mol Cell*. 2008;30:360-8.

28. Kleiger G and Mayor T. Perilous journey: a tour of the ubiquitin-proteasome system. *Trends Cell Biol*. 2014;24:352-9.
29. Groll M, Bajorek M, Kohler A, Moroder L, Rubin DM, Huber R, Glickman MH and Finley D. A gated channel into the proteasome core particle. *Nat Struct Biol*. 2000;7:1062-7.
30. Li Q. Advances in protein turnover analysis at the global level and biological insights. *Mass Spectrom Rev*. 2010;29:717-36.
31. Lau E, Cao Q, Ng DC, Bleakley BJ, Dincer TU, Bot BM, Wang D, Liem DA, Lam MP, Ge J and Ping P. A large dataset of protein dynamics in the mammalian heart proteome. *Sci Data*. 2016;3:160015.
32. Xu T, Park SK, Venable JD, Wohlschlegel JA, Diedrich JK, Cociorva D, Lu B, Liao L, Hewel J, Han X, Wong CC, Fonslow B, Delahunty C, Gao Y, Shah H and Yates JR, 3rd. ProLuCID: An improved SEQUEST-like algorithm with enhanced sensitivity and specificity. *J Proteomics*. 2015;129:16-24.
33. Gu ZC and Enenkel C. Proteasome assembly. *Cell Mol Life Sci*. 2014;71:4729-45.
34. Price JC, Guan S, Burlingame A, Prusiner SB and Ghaemmaghami S. Analysis of proteome dynamics in the mouse brain. *Proc Natl Acad Sci U S A*. 2010;107:14508-13.
35. Ghazalpour A, Rau CD, Farber CR, Bennett BJ, Orozco LD, van Nas A, Pan C, Allayee H, Beaven SW, Civelek M, Davis RC, Drake TA, Friedman RA, Furlotte N, Hui ST, Jentsch JD, Kostem E, Kang HM, Kang EY, Joo JW, Korshunov VA, Laughlin RE, Martin LJ, Ohmen JD, Parks BW, Pellegrini M, Reue K, Smith DJ, Tetradis S, Wang J, Wang Y, Weiss JN, Kirchgessner T, Gargalovic PS, Eskin E, Lusis AJ and LeBoeuf RC. Hybrid mouse diversity panel: a panel of inbred mouse strains suitable for analysis of complex genetic traits. *Mamm Genome*. 2012;23:680-92.
36. Im E and Chung KC. Precise assembly and regulation of 26S proteasome and correlation between proteasome dysfunction and neurodegenerative diseases. *BMB Rep*. 2016;49:459-73.

37. Murata S, Yashiroda H and Tanaka K. Molecular mechanisms of proteasome assembly. *Nat Rev Mol Cell Biol*. 2009;10:104-15.

38. Wang Z, Park K, Comer F, Hsieh-Wilson LC, Saudek CD and Hart GW. Site-specific GlcNAcylation of human erythrocyte proteins: potential biomarker(s) for diabetes. *Diabetes*. 2009;58:309-17.

39. Kimura Y, Takaoka M, Tanaka S, Sassa H, Tanaka K, Polevoda B, Sherman F and Hirano H. N(alpha)-acetylation and proteolytic activity of the yeast 20 S proteasome. *J Biol Chem*. 2000;275:4635-9.

40. Kulichkova VA, Tsimokha AS, Fedorova OA, Moiseeva TN, Bottril A, Lezina L, Gauze LN, Konstantinova IM, Mittenberg AG and Barlev NA. 26S proteasome exhibits endoribonuclease activity controlled by extra-cellular stimuli. *Cell Cycle*. 2010;9:840-9.

41. Mairinger FD, Walter RF, Theegarten D, Hager T, Vollbrecht C, Christoph DC, Worm K, Ting S, Werner R, Stamatis G, Mairinger T, Baba H, Zarogoulidis K, Huang H, Li Q, Tsakiridis K, Zarogoulidis P, Schmid KW and Wohlschlaeger J. Gene Expression Analysis of the 26S Proteasome Subunit PSMB4 Reveals Significant Upregulation, Different Expression and Association with Proliferation in Human Pulmonary Neuroendocrine Tumours. *J Cancer*. 2014;5:646-54.

42. Jin YC, Li ZH, Hong ZS, Xu CX, Han JA, Choi SH, Yin JL, Zhang QK, Lee KB, Kang SK, Song MK, Kim YJ, Kang HS, Choi YJ and Lee HG. Conjugated linoleic acid synthesis-related protein proteasome subunit alpha 5 (PSMA5) is increased by vaccenic acid treatment in goat mammary tissue. *J Dairy Sci*. 2012;95:4286-97.

43. Sebens S, Bauer I, Geismann C, Grage-Griebenow E, Ehlers S, Kruse ML, Arlt A and Schafer H. Inflammatory macrophages induce Nrf2 transcription factor-dependent proteasome activity in colonic NCM460 cells and thereby confer anti-apoptotic protection. *J Biol Chem*. 2011;286:40911-21.

44. Caputi FF, Carboni L, Mazza D, Candeletti S and Romualdi P. Cocaine and ethanol target 26S proteasome activity and gene expression in neuroblastoma cells. *Drug Alcohol Depend*. 2016;161:265-75.
45. Waller-Evans H, Hue C, Fearnside J, Rothwell AR, Lockstone HE, Calderari S, Wilder SP, Cazier JB, Scott J and Gauguier D. Nutrigenomics of high fat diet induced obesity in mice suggests relationships between susceptibility to fatty liver disease and the proteasome. *PLoS One*. 2013;8:e82825.
46. Obermann WM, Sondermann H, Russo AA, Pavletich NP and Hartl FU. In vivo function of Hsp90 is dependent on ATP binding and ATP hydrolysis. *J Cell Biol*. 1998;143:901-10.
47. Gething MJ and Sambrook J. Protein folding in the cell. *Nature*. 1992;355:33-45.
48. Hong DS, Banerji U, Tavana B, George GC, Aaron J and Kurzrock R. Targeting the molecular chaperone heat shock protein 90 (HSP90): lessons learned and future directions. *Cancer Treat Rev*. 2013;39:375-87.
49. Jhaveri K, Taldone T, Modi S and Chiosis G. Advances in the clinical development of heat shock protein 90 (Hsp90) inhibitors in cancers. *Biochim Biophys Acta*. 2012;1823:742-55.
50. Den RB and Lu B. Heat shock protein 90 inhibition: rationale and clinical potential. *Ther Adv Med Oncol*. 2012;4:211-8.
51. Garcia R, Merino D, Gomez JM, Nistal JF, Hurle MA, Cortajarena AL and Villar AV. Extracellular heat shock protein 90 binding to TGFbeta receptor I participates in TGFbeta-mediated collagen production in myocardial fibroblasts. *Cell Signal*. 2016;28:1563-79.
52. Grabek KR, Karimpour-Fard A, Epperson LE, Hindle A, Hunter LE and Martin SL. Multistate proteomics analysis reveals novel strategies used by a hibernator to precondition the heart and conserve ATP for winter heterothermy. *Physiol Genomics*. 2011;43:1263-75.
53. Tang L and Taylor PB. Altered contractile function in isoproterenol-induced hypertrophied rat heart. *J Hypertens*. 1996;14:751-7.

54. Rauniyar N and Yates JR, 3rd. Isobaric labeling-based relative quantification in shotgun proteomics. *J Proteome Res*. 2014;13:5293-309.

55. Sulistio YA and Heese K. The Ubiquitin-Proteasome System and Molecular Chaperone Deregulation in Alzheimer's Disease. *Mol Neurobiol*. 2016;53:905-31.

56. Ortega Z and Lucas JJ. Ubiquitin-proteasome system involvement in Huntington's disease. *Front Mol Neurosci*. 2014;7:77.

57. Ikeda K, Akiyama H, Arai T, Ueno H, Tsuchiya K and Kosaka K. Morphometrical reappraisal of motor neuron system of Pick's disease and amyotrophic lateral sclerosis with dementia. *Acta Neuropathol*. 2002;104:21-8.

58. Karin M and Delhase M. The I kappa B kinase (IKK) and NF-kappa B: key elements of proinflammatory signalling. *Semin Immunol*. 2000;12:85-98.

59. Ermolaeva MA, Dakhovnik A and Schumacher B. Quality control mechanisms in cellular and systemic DNA damage responses. *Ageing Res Rev*. 2015;23:3-11.

60. Calise J and Powell SR. The ubiquitin proteasome system and myocardial ischemia. *Am J Physiol Heart Circ Physiol*. 2013;304:H337-49.

61. Sandri M and Robbins J. Proteotoxicity: an underappreciated pathology in cardiac disease. *J Mol Cell Cardiol*. 2014;71:3-10.

62. Majetschak M. Regulation of the proteasome by ATP: implications for ischemic myocardial injury and donor heart preservation. *Am J Physiol Heart Circ Physiol*. 2013;305:H267-78.

63. Powell SR. The ubiquitin-proteasome system in cardiac physiology and pathology. *Am J Physiol Heart Circ Physiol*. 2006;291:H1-H19.

64. Li J, Ma W, Yue G, Tang Y, Kim IM, Weintraub NL, Wang X and Su H. Cardiac proteasome functional insufficiency plays a pathogenic role in diabetic cardiomyopathy. *J Mol Cell Cardiol*. 2017;102:53-60.